

Momentum Distribution of Near-Zero-Energy Photoelectrons in the Strong-Field Tunneling Ionization in the Long Wavelength Limit

Q. Z. Xia,¹ D. F. Ye,¹ L. B. Fu,^{1,*} X. Y. Han,¹ and J. Liu^{1,2,†}

¹National Laboratory of Science and Technology on Computational Physics,

Institute of Applied Physics and Computational Mathematics, Beijing 100088, China

²HEDPS, Center for Applied Physics and Technology, Peking University, Beijing 100084, China

We investigate the ionization dynamics of Argon atoms irradiated by an ultrashort intense laser of a wavelength up to 3100 nm, addressing the momentum distribution of the photoelectrons with near-zero-energy. We find a surprising accumulation in the momentum distribution corresponding to meV energy and a “V”-like structure at the slightly larger transverse momenta. Semiclassical simulations indicate the crucial role of the Coulomb attraction between the escaping electron and the remaining ion at extremely large distance. Tracing back classical trajectories, we find the tunneling electrons born in a certain window of the field phase and transverse velocity are responsible for the striking accumulation. Our theoretical results are consistent with recent meV-resolved high-precision measurements.

PACS numbers: 32.30.-r,32.80.Fb,33.60.-q,31.15.Ar

Introduction—The above-threshold ionization (ATI) phenomenon of atoms exposed to a strong field has attracted sustaining attention for decades since it was first discovered in 1979 [1]. One of the most pronounced features of the ATI in the long-wavelength limit, is the high-energy photoelectron spectrum plateau extending up to $10U_P$ ($U_P = I/4\omega^2$, denotes the ponderomotive energy, where I is the laser intensity and ω the frequency in atomic units) [2]. The underlying mechanism has been attributed to the tunneled electron’s multiple return and rescattering by its parent ion [3–7].

Recently, some unexpected low-energy structures (LES) of ATI [8–10] were observed in the tunneling regime, initially at several eV and then at lower energies of less than 1eV, triggering a new surge of attention of ATI. Although from all aspects, including quantum and semiclassical, numerous theoretical investigations [8–17] of the underlying physics of the LES were reported, the controversies on the surprising structure have been continuing. In the above experiments, the photoelectrons are detected only in a small angle around the laser polarization direction by a time-of-flight spectrometer. Because the LES is subtle and sensitive, it is difficult to disentangle the origin of the various findings without large solid angle measurements including momentum information with high resolution. Recent experimental work by J. Dura *et al* [18] steps forward in this direction. In the experiment, with a specifically developed ultrafast mid-IR light source of 3100 nm in the combination with a 3D reaction microscope, the strong-field dynamics is explored in three-dimensional momentum space down to meV electron energies with an unprecedented precision [18]. Instead of structures on the eV level, an apparent meV electron accumulation in the ATI spectrum and a striking momentum distribution for the near-zero-energy electron are observed. Nevertheless, the physics underlying the meV electron distribution is unsettled that calls

for an investigation from theoretical side urgently.

In this Letter, stimulated by the recent experiment and attempting to resolve the controversies on LES, we theoretically investigate the ionization dynamics of Argon atoms by intense laser fields in the deep tunneling regime of $\gamma \ll 1$ (Keldysh parameter $\gamma = \sqrt{I_p/2U_p}$, where I_p is the ionization potential), with special emphasis on addressing the low momentum distribution of the near-zero-energy photoelectrons. Our study is facilitated by an improved semiclassical rescattering model that includes the Coulomb attraction and trajectory interference and can precisely produce the momenta of the near-zero-energy photoelectrons regardless of the Coulomb long-range tail. Our theory accounts the surprising accumulation around near-zero momenta corresponding to meV energies and predicts a “V”-like structure at slightly larger transverse momenta. We identify the roles of the Coulomb attraction and trajectory interference, by tracing back the trajectories of soft and chaotic scattering, respectively. Our work provides profound insight into the meV low-energy ATI mechanism, and combined with the recent high-precision experimental results can help unraveling the debate about the LES.

Model—In the semiclassical model, the atomic ionization consists two essential physical processes, i.e., an electron tunnels through the Coulomb field that has been dramatically suppressed by the laser field, and the released electron is driven by laser field to scatter with its parent ion [6]. The tunneled electrons (released at a distance r_0 from the ion) have initially zero longitudinal velocity and a Gaussian transverse velocity distribution. Each trajectory is weighed by the ADK ionization rate $\varpi(t_0, v_{\perp}^i) = \varpi_0(t_0)\varpi_1(v_{\perp}^i)$ [19], where $\varpi_1(v_{\perp}^i) = (2\sqrt{2I_p}v_{\perp}^i/|\varepsilon(t_0)|) \exp[-\sqrt{2I_p}(v_{\perp}^i)^2/|\varepsilon(t_0)|]$ is the distribution of initial transverse velocity, and $\varpi_0(t_0) = |\varepsilon(t_0)|^{(1-2/\sqrt{2I_p})} \exp[-2(2I_p)^{3/2}/|3\varepsilon(t_0)|]$, depending on the field phase ωt_0 at the instant of tunnel-

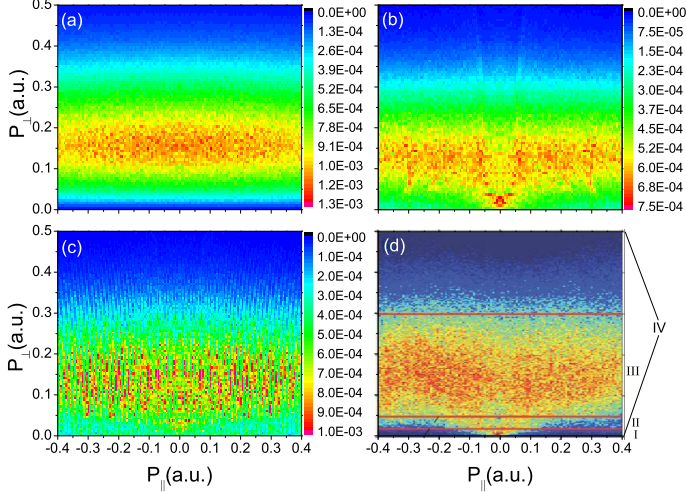


FIG. 1: (Color online) (a) Momentum distribution calculated from the model without considering the Coulomb attraction in rescattering; (b) Results from the model with considering the Coulomb attraction; (c) The results with considering both Coulomb field and trajectory interference; (d) Momentum spectrum from experiment cited from [18] for comparison.

ing as well as on the ionization potential I_p . In the post-tunneling process, the electron evolution in the combined oscillating laser field and Coulomb field is traced via the classical Newtonian equation $d^2\vec{r}/dt^2 = -\vec{r}/r^3 - \vec{\varepsilon}(t)$. The physical quantities can then be calculated through weighted averaging over the ensemble of trajectories corresponding to diverse initial laser phases and transverse velocities at tunneling.

We have made simulations for Ar atoms with $I_p = 0.583$ a.u.. The laser parameters are chosen as $\varepsilon_0 = 0.053$ a.u. and $\omega = 0.0147$ a.u. ($\lambda = 3100$ nm) to match the experiment [18]. Thus, the Keldysh parameter $\gamma = 0.3$. The pulse envelope is half-trapezoidal, constant for the first six cycles and ramped off within the last six cycles. After the laser pulse is over, the instantaneous positions and momenta of the emitted electrons are recorded. However, the instantaneous momenta are not equal to the asymptotic ones (i.e., $r \rightarrow \infty$) collected by a detector due to the Coulomb long-range tail. To precisely reproduce the near-zero momentum distribution, we need to extract the asymptotic momenta from the instantaneous positions and momenta. The Coulomb two-body system has two conserved vectors: the angular momentum $\vec{M} = \vec{r} \times \vec{p}$ and the Laplace-Runge-Lenz vector $\vec{A} = \vec{p} \times \vec{M} - \vec{r}/r$. Using the conserved quantities and after some coordinate rotations, we can then obtain the asymptotic momenta of the emitted electrons.

The above classical trajectory evolution, however, ignore the quantum interference totally. To retrieve the interference effect, we assign a phase to each trajectory.

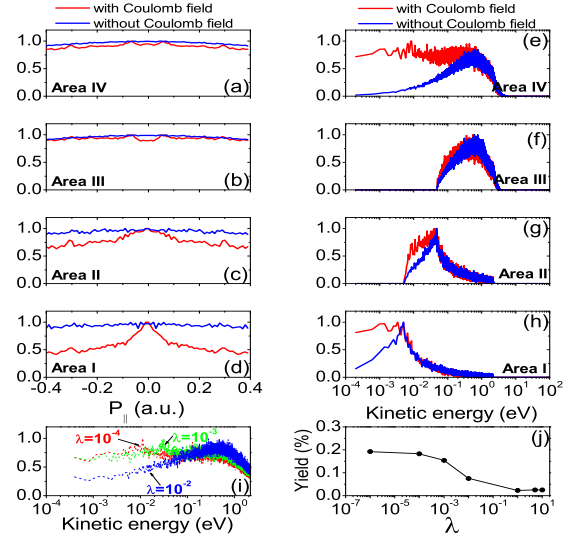


FIG. 2: (Color online)(a)-(h)The parallel momentum distribution and the energy distribution counted from Fig. 1(b), with respect to the four areas within the momentum map of Fig. 1(d). (a) and (e) correspond to the area IV; (b) and (f) correspond to the area III; (c) and (g) to the area II; and (d) and (h) to the area I. Red curves denote the results of the semiclassical simulation with the Coulomb field, while the blue ones represent the simulation results without the Coulomb field. (i) and (j) are simulation results from screening potentials: (i) Low energy distribution with respect to screening parameters; (j) meV photoelectron yields vs. the screening parameters.

The phase S is determined by the integral $S(t_0, v_{\perp}^i) = -i \int_{t_0}^{t_f} [\frac{1}{2} \vec{v}^2(t) - \frac{1}{r(t)} + I_p] dt$ [17], here $\vec{v}(t)$ and $r(t)$ is the solution of the Newton equation with the initial condition t_0 , v_{\perp}^i and tunneling position r_0 . Then, the transition amplitude from the initial state to the continuum state with the asymptotic momentum $(p_{\parallel}, p_{\perp})$ can be calculated as $M(p_{\parallel}, p_{\perp}) = \sum_{t_0, v_{\perp}^i} \sqrt{\varpi(t_0, v_{\perp}^i)} \exp[S(t_0, v_{\perp}^i)]$, where the summation includes all the trajectories leading to the same final momentum $(p_{\parallel}, p_{\perp})$. The momentum spectra can be obtained from $|M(p_{\parallel}, p_{\perp})|^2$. Here, we only consider the electrons released within the first cycle ($\omega t_0 \in [0, 2\pi]$). In our simulation, more than 5 million trajectories are calculated and the convergence of the results has been tested by increasing the number of trajectories.

Momentum Distribution of Low-Energy Electrons— Fig. 1 (a) (b) and (c) show our model calculations on the momentum distribution spectra of low-energy electrons in the momentum ranges $p_{\parallel} \in (-0.4, 0.4)$ and $p_{\perp} \in (0, 0.5)$, indicating the prominent roles of both the Coulomb potential and trajectory interference.

We can first see the important role of the Coulomb attraction by comparing Fig. 1(a) and (b). In Fig. 1(a), we artificially remove the Coulomb potential in the post-

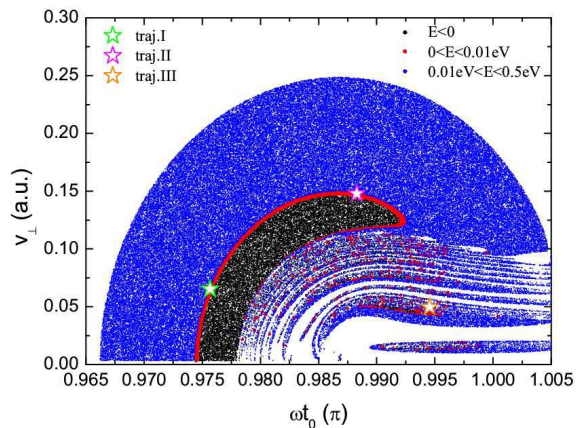


FIG. 3: (Color online) The dependence of final kinetic energy on tunneling time and initial transverse velocity around peak field. The data are plotted in different colors with respect to different electron energy ranges. The blank areas contribute to high-energy electrons with $E > 0.5\text{eV}$, which are not in the focus of the present discussion.

tunneling scattering. Here, the momentum spectrum exhibits a simple “sandwich”-like structure, with the dense distribution in the central belt only reflecting the Gaussian type distribution of initial transverse velocities. In this case, we can not see any accumulation near zero momentum. However, in the presence of the Coulomb potential (see Fig. 1 (b)), we can obviously observe the accumulation near zero momentum as well as a “V”-like structure at the slightly larger transverse momenta.

The role of the trajectory interference becomes obvious when comparing Fig. 1 (c) and (b): The dense belt structure broadens and the accumulation near origin fades out a little, in better agreement with the experiment. Fig. 1(c) also shows fine vertical interference contrasts.

To achieve deeper insight into the origin of the striking structure in the momentum distribution and address its relation to the energy spectrum, we take average the transverse momentum and generate energy distributions with respect to distinct transverse momentum regimes, i.e., accumulation regime (I), V-structure regime (II), and belt regime (III). Symbol IV represents the sum over the above three regimes. In our energy statistics, the energy interval is chosen as 0.4 meV, consistent with the experimental resolution. The results are shown in Fig. 2.

From Fig. 2 (f) to (h), we see the Coulomb effects increase and become very significant at small transverse velocities. The envelope of the total energy spectrum (e) shows a prominent hump around 0.5 eV and then extends to meV energies or even less. The hump is also apparent in experiment [18]. Nevertheless, it has nothing to do with the Coulomb attraction, is just due to momentum space density compression when transformed to energy distribution. An estimation of the hump center is given by $\partial\varpi(t_0, v_{\perp}^i)/\partial t_0 = 0$ and $\partial\varpi(t_0, v_{\perp}^i)/\partial v_{\perp}^i = 0$. In the

long-wavelength limit of $\omega \rightarrow 0$, we analytically obtain an electron kinetic energy of $\varepsilon_0/4\sqrt{2I_p}$, here ε_0 is the maximum field strength. Substituting the atom and laser parameters, it gives 0.33 eV, in close agreement with the results of the simulation. In contrast to the experiment, below the hump, our simulation exhibits a plateau structure in energy spectrum that spreads down the regime of 10^{-4} eV or less.

The meV electrons are closely related to the Coulomb attraction. In particular, we find that the long-range Coulomb attraction between the electron and ion plays a crucial role, in contrast to the Coulomb focusing effect [20] that is significant only when the electron is closer to ion. We have replaced the Coulomb potential by a Yukawa type potential of $-exp[-\lambda r]/r$, to screen the Coulomb long-range tail (see Fig. 2 (i) and (j)). We find surprisingly that, even with a very small screening parameter of $\lambda = 0.01$, the meV electron yield decreases rapidly, analogous to the case where the Coulomb potential is completely absent. Only with much smaller screening parameters of 0.001 or less, the meV electron accumulation can recover. The above observation unambiguously indicates the crucial role of the Coulomb attraction between the escaping electron and ion at the extremely long distance ($\gg 100$ a.u.), and provides the strong evidence that the highly excited Rydberg states are involved in the meV electron dynamics. We have also calculated the meV electron yields (i. e. energy less than 0.01 eV) with respect to the screening parameters in Fig. 2 (j), which mainly exhibits a logarithm feature. The singularity stemmed from the Coulomb long tail also emerges in heavy ion impact ionization with manifesting a sharp cusp-like peak at zero transverse momentum [21]. Recently, the cutoff of Coulomb potential at the distance of a few atomic units is found to affect the momentum spectra of the electrons with eV energy in multiphoton regime [22, 23]. Here, we find that the tiny Coulomb tail at distance much larger than 100 a.u. can significantly help producing the meV photoelectrons and lead to the striking distribution in momentum spectrum.

The striking meV electron accumulation is found to be dependent on laser wavelength. We have extended our simulations to shorter wavelength of 800 nm and find that apparent accumulation around near-zero momenta become less visible. This is due to the stabilization of the high-excited Rydberg states that are deeply involved in the meV photoelectron dynamics. When field frequency is much larger than the Rydberg orbit frequency, the electrons that are pumped into the Rydberg states become stabilized against ionization [24, 25]. This effect can reduce the meV electron accumulation. Actually, we have simply estimated the most possible energy of the electrons that are pumped by the laser field. According to the zero origin of the energy, we can obtain a critical Keldysh parameter of $\gamma_c = (\sqrt{I_p}/2\sqrt{2})^{1/2}$, below which the most possible electron energy shifts to a positive value

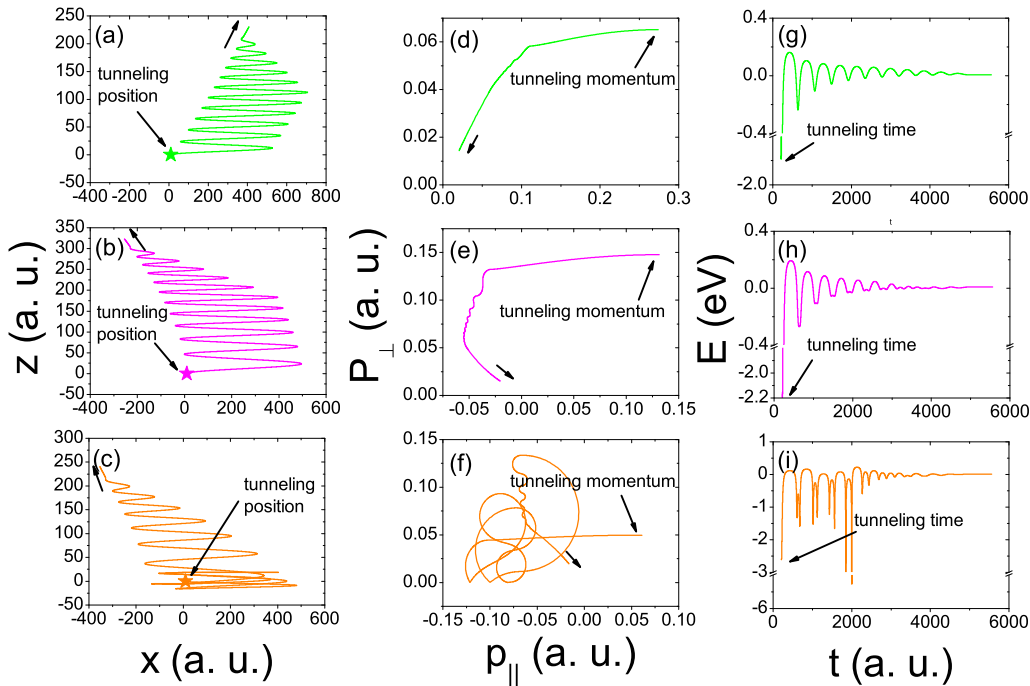


FIG. 4: (Color online) Three typical trajectories leading to meV energy and their corresponding temporal evolutions of the momentum and energy. (a) (d) and (g), the soft forward scattering trajectory; (b) (e) and (h), the soft backward scattering; (c) (f) and (i), the chaotic scattering.

indicating the emergence of the hump structure similar to Fig. 2(e). We therefore predict that the surprising meV electron accumulation around near-zero momenta should be universal in the deep tunneling regime of $\gamma < \gamma_c$. This is the case for the present experiment [18], where $\gamma = 0.3$ and the critical Keldysh parameter for Ar atom is around 0.5.

Classical Trajectory Analysis of the source of the meV electrons—In our semiclassical model, the emitted electron’s energy is determined by the tunneling time and initial perpendicular velocity. In Fig. 3, we show the dependence of the final kinetic energy on the tunneling time and initial transverse velocity around peak field. The meV electrons originate from the red area that consists of a regular arc region and scattered irregular regions below the arc. The irregular zone is self-similar and has fractal properties [6, 26–28]. The trajectories originated from this region might experience multiple returns to the ion and the final energies is very sensitive to the initial conditions. The chaotic multiple rescatterings by the Coulomb field might lead to extremely high energy electrons that are responsible for the well-known ATI plateau structure [6]. It can also result in extremely low-energy electrons, as shown by the scattered red dots below the arc region.

Besides these chaotic trajectories, we find the electrons

with meV energy usually experience soft scattering and then move forward or backward [12, 17]. We plot such three kinds of typical trajectories in Fig. 4 (a), (b) and (c), respectively. Their initial conditions correspond to the “stars” in Fig. 3. Temporal evolution of the momenta and energy for each trajectory is shown in Fig. 4(d-f) and (g-i), respectively. Since the electrons oscillate in the laser field, here we use the compensated energy [29] calculated via the canonical momentum instead of the kinetic energy. Fig. 4 (a) (g) and (b) (h) indicate that, some electrons originated in a certain window of laser phase and initial transverse velocity can tunnel into Rydberg states without ionization. They locate far away from the parent ion and are weakly bounded by the ion’s Coulomb attraction. They subsequently experience very soft rescattering during which they can only acquire limited field energy to be pumped into the continuum with meV energy. During the process, the Coulomb potential attracts the electron that reduces the electron’s tunneling momentum to zero showing a kind of “friction” effect (see Fig. 4 (d) and (e)). While for the chaotic trajectory, the electrons experience multiple scatterings with ion and “occasionally” emit with meV energy. Our model calculation indicates both chaotic and soft (forward or backward) recattering trajectories are the source of meV

photoelectrons and the ratio of the two kinds events (i.e., chaotic events vs. soft rescattering events) is about 1/4.

In summary, we have investigated the dynamics of meV ATI photoelectrons from theoretical side for the first time. Our simulations indicate that the meV electron generation is subtle and attributed to the extremely long-range Coulomb tail, while it is also of universality in the deep tunneling regime. Our theoretical results account for the recent high-precision ATI experiments and some predictions are given that calls for the verification from further experiments. Since the meV energy corresponds to terahertz, the present results can also have implications in the generation of terahertz radiation [30].

This work is supported by the National Fundamental Research Program of China (Contact No 2011CB921503, 2013CBA01502, and 2013CB83410), the NNSF of China (Contact Nos. 11274051, 11374040, 11078001,10933001).

* Electronic address: lbfu@iapcm.ac.cn

† Electronic address: liu'jie@iapcm.ac.cn

- [1] P. Agostini, F. Fabre, G. Mainfray, and G. Petite, Phys. Rev. Lett. **42**, 1127 (1979).
- [2] G. G. Paulus *et.al.*, Phys. Rev. Lett. **72**, 2851 (1994); B. Walker, B. Sheehy, K. C. Kulander, and L. F. DiMauro, Phys. Rev. Lett. **77**, 5031 (1996).
- [3] P. B. Corkum, Phys. Today **64**, 36 (2011).
- [4] P. B. Corkum, N. H. Burnett, and F. Brunel, Phys. Rev. Lett. **62**, 1259 (1989); K. J. Schafer, Baorui Yang, L. F. DiMauro, and K. C. Kulander, Phys. Rev. Lett. **70**, 1599 (1993); P. B. Corkum, Phys. Rev. Lett. **71**, 1994 (1993); G. G. Paulus, W. Becker, W. Nicklich and H. Walther, J. Phys. B **27**, L703 (1994).
- [5] D. B. Milosevic and W. Becker, Phys. Rev. A **68**, 065401 (2003).
- [6] B. Hu and J. Liu and S. G. Chen, Phys. Lett. A **236**, 533 (1997).
- [7] X. M. Tong, S. Watahiki, K. Hino, and N. Toshima, Phys. Rev. Lett. **99**, 093001 (2007).
- [8] C. I. Blaga *et.al.*, Nat. Phys. **5**, 335 (2009).
- [9] W. Quan *et.al.*, Phys. Rev. Lett. **103**, 093001 (2009).
- [10] C. Y. Wu, *et al.*, Phys. Rev. Lett. **109**, 043001 (2012).
- [11] C. Liu and K. Z. Hatsagortsyan, Phys. Rev. Lett. **105**, 113003 (2010).
- [12] A. Kästner, U. Saalmann and J. M. Rost, Phys. Rev. Lett. **108**, 033201 (2012).
- [13] I. Burenkov, A. Popov, O. Tikhonova, E. Volkova, Laser Phys. Lett. **108**, ARTN033201 (2010).
- [14] C. Lemell *et.al.*, Phys. Rev. A **85**, 011403 (2012).
- [15] F. Catoire *et.al.*, Laser Phys. **19**, 1674 (2009).
- [16] F. H. M. Faisal, Nat. Phys. **5**, 319 (2009).
- [17] T. M. Yan, S. V. Popruzhenko, M. J. J. Vrakking, and D. Bauer, Phys. Rev. Lett. **105**, 253002 (2010).
- [18] J. Dura, N. Camus, A. Thai, A. Britz, M. Hemmer, M. Baudisch, A. Senftleben, C. D. Schroter, J. Ullrich, R. Moshhammer and J. Biegert, Scientific Reports **3**, 2675 (2013)
- [19] A. M. Perelomov, V. S. Popov, and V. M. Terent'ev, Zh. Eksp. Teor. Fiz. **52**, 514 (1967) [Sov. Phys. JETP **25**, 336 (1967)]; M. V. Ammosov, N. B. Delone, and V. P. Krainov, Zh. Eksp. Teor. Fiz. **91**, 2008 (1986) [Sov. Phys. JETP **64**, 1191 (1986)]; N. B. Delone and V. P. Krainov, J. Opt. Soc. Am. B **8**, 1207 (1991).
- [20] T. Brabec, M. Yu., and Paul B. Corkum, Phys. Rev. A **54**, R2551–R2554 (1996).
- [21] J. Macek, Phys. Rev. A **1** 235 (1970); J. Burgdörfer, Phys. Rev. Lett. **51** 374 (1983).
- [22] A. Rudenko, K. Zrost, Th. Ergler, A.B. Voitkiv, B. Najjari, V. L. B. de Jesus, B. Feuerstein, C. D. Schroter, R. Moshhammer, and J. Ullrich, J. Phys. B: At. Mol. Opt. Phys. **38** (2005) L191.
- [23] Z.Chen, T.Morishita, A. T. Le, M. Wickenhauser, X. M. Tong, and C. D. Lin, Phys. Rev. A **74**, 053405 (2006).
- [24] H. Liu, *et al*, Phys. Rev. Lett. **109**, 093001 (2012).
- [25] K. Y. Huang, Q. Z. Xia, and L. B. Fu Phys. Rev. A **87**, 033415 (2013).
- [26] Edward Ott, 'Chaos in Dynamical System', Cambridge Univ. Press, (1993).
- [27] G. van de Sand and J. M. Rost, Phys. Rev. Lett. **83**, 524 (1999).
- [28] L. B. Fu, G. G. Xin, D. F. Ye, and J. Liu, Phys. Rev. Lett. **108**, 103601 (2012).
- [29] J. G. Leopold and I. C. Percival, J. Phys. B, **12**, 709 (1979).
- [30] Z. Y. Zhou, *et. al.*, Phys. Rev. A **79**, 063413 (2009); B. Zhou, et al, Phys. Rev. Lett. **106**, 255002 (2011).